REPORT

SOLAR CELLS

Liquid medium annealing for fabricating durable perovskite solar cells with improved reproducibility

Nengxu Li[1,2]†, Xiuxiu Niu[1,2]†, Liang Li[2], Hao Wang[1,3], Zijian Huang[2], Yu Zhang[2], Yihua Chen[2], Xiao Zhang[1], Cheng Zhu[1], Huachao Zai[2], Yang Bai[1], Sai Ma[1], Huifen Liu[2], Xixia Liu[2], Zhenyu Guo[2], Guilin Liu[4], Rundong Fan[2], Hong Chen[5], Jianpu Wang[5], Yingzhuo Lun[6], Xueyun Wang[6], Jiawang Hong[6], Haipeng Xie[7], Devon S. Jakob[8], Xiaoji G. Xu[8], Qi Chen[1]*, Huanping Zhou[2]*

Solution processing of semiconductors is highly promising for the high-throughput production of cost-effective electronics and optoelectronics. Although hybrid perovskites have potential in various device applications, challenges remain in the development of high-quality materials with simultaneously improved processing reproducibility and scalability. Here, we report a liquid medium annealing (LMA) technology that creates a robust chemical environment and constant heating field to modulate crystal growth over the entire film. Our method produces films with high crystallinity, fewer defects, desired stoichiometry, and overall film homogeneity. The resulting perovskite solar cells (PSCs) yield a stabilized power output of 24.04% (certified 23.7%, 0.08 cm^2) and maintain 95% of their initial power conversion efficiency (PCE) after 2000 hours of operation. In addition, the 1-cm^2 PSCs exhibit a stabilized power output of 23.15% (certified PCE 22.3%) and keep 90% of their initial PCE after 1120 hours of operation, which illustrates their feasibility for scalable fabrication. LMA is less climate dependent and produces devices in-house with negligible performance variance year round. This method thus opens a new and effective avenue to improving the quality of perovskite films and photovoltaic devices in a scalable and reproducible manner.

Solution processing of semiconductors is a promising approach for the fabrication of cost-effective electronics and optoelectronics (*1*, *2*). Recently, metal halide perovskites based on a solution process have been shown to have electronic and optoelectronic properties applicable in various device applications, particularly photovoltaics (PV) (*3*–*6*). These perovskites have reached a power conversion efficiency (PCE) of 25.5% within just one decade of research (*7*) and are therefore regarded as promising candidates for next-generation PV. Reviewing the development of this family of materials, early investigations of device physics revealed that the perovskite crystal quality (e.g., crystallinity, morphology, stoichiometry, etc.) profoundly influenced cell and module efficiencies (*8*, *9*). The operational lifetime of high-efficiency cells has been prolonged to several thousand hours during accelerated aging tests, gradually approaching the requirements for practical use (*10*). In the context of device aging courses, the crystal quality again has become a research focus with an emphasis on its time evolution (*11*), which is governed by thermodynamic and kinetic factors, including components, chemical potential, structure, phase transition and segregation, ion migration, and defect concentrations (*10*).

To promote the commercialization of perovskite PV, it is important to develop a scalable solution process with sufficient reproducibility. Research should expand the investigation of crystal quality in the spatial perspective (*12*), aiming at precise control of perovskite crystallization kinetics over the entire film at any atmosphere. However, there will be substantial difficulties in achieving this. First, perovskite formation includes a reaction between Lewis acids and bases that occurs quickly and spontaneously even at low temperature (*13*). Second, halide perovskites for practical use are often mixtures (*14*) in which the different components exhibit different reactivity and diffusivity during film growth. In addition, the precursor reactants are sensitive to moisture and common solvents (*15*, *16*), which leads to considerable variance with each slight change in processing conditions.

High-quality crystalline perovskite films generally have a large grain size, which is achieved by retarding nucleation and promoting crystal growth according to the LaMer model (*17*). Several strategies have been successfully applied to decrease the nucleation rate (*18*, *19*), which effectively influences crystallization kinetics. In addition, higher annealing temperature and/or prolonged annealing time are reported to increase the crystallinity of perovskites by increasing crystal growth rate or inducing a recrystallization process (*20*, *21*). However, coincident defects caused by unfavorable volatile component loss are often found, accompanied by substantial inhomogeneity in the film over a larger area (*22*, *23*). Moreover, local fluctuations in processing atmosphere leads to films with varied quality (*15*, *16*) and thus poor reproducibility. Therefore, it is challenging to develop a simple, controllable, and effective annealing technology that meets the requirements for scalable and reproducible fabrication.

Here, we demonstrate liquid medium annealing (LMA) as a method of effectively modulating the crystal growth of halide perovskite materials. Rather than merely raising the annealing temperature, LMA adopts omnidirectional heating, particularly an extra "top-down" heat transfer on the film to accelerate crystal growth with a higher heating rate. In addition, the liquid medium extracts residual solvents from precursor films to mitigate their disturbance for crystal growth. Moreover, the liquid medium creates a microenvironment for crystal growth to prevent volatile component loss from the desired stoichiometry over the entire film. Consequently, LMA leads to excellent film homogeneity, which is also less dependent on the processing atmosphere and applicable for all-weather in-house fabrication. Small-area devices (0.08 cm^2) using LMA exhibited a stabilized power output of 24.04% (certified 23.7%) and maintained 95% of their initial PCE after 2000 hours of stabilized power output (SPO) tracking. The corresponding large-area solar cells (1 cm^2) achieved a stabilized power output of 23.15% (certified PCE of 22.3%) and kept 90% of their original PCE after 1120 hours of SPO tracking. To our knowledge, this is the smallest efficiency gap between small- and large-area devices ever reported. Our findings provide a reproducible technology with which to fabricate high-quality and homogeneous perovskite films for the production of efficient and stable large-area solar cells or other perovskite-based optoelectronics.

Fine control on the annealing process, especially in the early stage, is crucial to modulating the crystallization dynamics and quality of perovskite films. In contrast to most annealing technologies, which are generally performed under certain atmosphere, we used LMA to fabricate perovskite films in which the as-deposited film is annealed in the preheated

[1]Experimental Centre for Advanced Materials, School of Materials Science and Engineering, Beijing Institute of Technology, Beijing 100081, P. R. China. [2]Beijing Key Laboratory for Theory and Technology of Advanced Battery Materials, Key Laboratory of Polymer Chemistry and Physics of Ministry of Education, BIC-ESAT, School of Materials Science and Engineering, Peking University, Beijing 100871, P. R. China. [3]Beijing Institute of Technology Chongqing Innovation Centre, Chongqing 401120, P. R. China. [4]School of Science, Jiangnan University, Wuxi, Jiangsu 214122, P. R. China. [5]Key Laboratory of Flexible Electronics (KLOFE) and Institute of Advanced Materials (IAM), Nanjing Tech University (NanjingTech), Nanjing 210009, P. R. China. [6]School of Aerospace Engineering, Beijing Institute of Technology, Beijing 100081, P. R. China. [7]Hunan Key Laboratory for Super-microstructure and Ultrafast Process, School of Physics and Electronics, Central South University, Changsha, Hunan 410012, P.R. China. [8]Department of Chemistry, Lehigh University, Bethlehem, PA 18015, USA.
*Corresponding author. Email: qic@bit.edu.cn (Q. C.); happy_zhou@pku.edu.cn (H. Zhou)
†These authors contributed equally to this work.

liquid (Fig. 1A). The liquid medium in use (anisole in this work) needs to exhibit a high thermal conductivity and low viscosity with the appropriate organic solvent extraction ability but negligible reactivity with perovskites. Different from the traditional annealing (Ref) method, LMA (Fig. 1B) uses the liquid to transfer heat and create a reaction microenvironment that produces substantially different crystallization dynamics of perovskite films mainly by affecting the heating mode and solvated intermediates.

In traditional annealing, heating is "bottom-up," meaning that heat transfers from hotplate to glass substrate to perovskite films (Fig. 1D). This results in delayed heating at the film surface, where the directional crystallization has already begun (*24*). This heating transfer is in the opposite direction from crystallization, which may impede the crystal growth because of the limited diffusion of the reactants. LMA provides omnidirectional heating, in particular an extra "top-down" heat transfer, which allows fast heating of the film surface once it is in contact with the hot liquid (Fig. 1C). This top-down heating mode is in line with the crystal growth direction of perovskite polycrystalline films.

To illustrate the heating mode, we performed finite element analysis to simulate the thermal field and the annealing time in two processes (Fig. 2, A and B). Keeping the heat source at 150°C, the Ref film required ~13 s to reach 140°C at equilibrium upon bottom-up annealing (Fig. 2A). The retarded heating rate was attributed to the heat transfer delay of glass and the considerable thermal convection between perovskite and air. By contrast, the perovskite film by LMA took only ~4 s to reach 141°C (Fig. 2B) because the top-down heating mode allowed immediate heating of the entire perovskite film in a hot liquid. In addition, the liquid medium could form a relatively stable thermal field on perovskite films by avoiding unfavorable thermal convection with air. We investigated the temperature evolution in perovskite films and found that LMA exhibited a much faster heating rate of 32.7°C/s compared with that of Ref at 8.7°C/s (Fig. 2C). Also, the temperature variation along the vertical direction of perovskite film was negligible for annealing (Fig. 2C, inset) because of the extremely thin thickness of the film compared with the substrate. Overall, the higher heating rate in the initial stage could potentially accelerate the diffusion of reactants (such as organic cations, Pb-I octahedra, etc.) and thus promote the grain growth rate, which will be discussed later.

Anisole is an ideal liquid medium for perovskite fabrication because of its high thermal conductivity (0.137 W/m K) and relatively low viscosity (0.99 mPa/s at 20°C). In addition, it has a poor solubility in water but is miscible

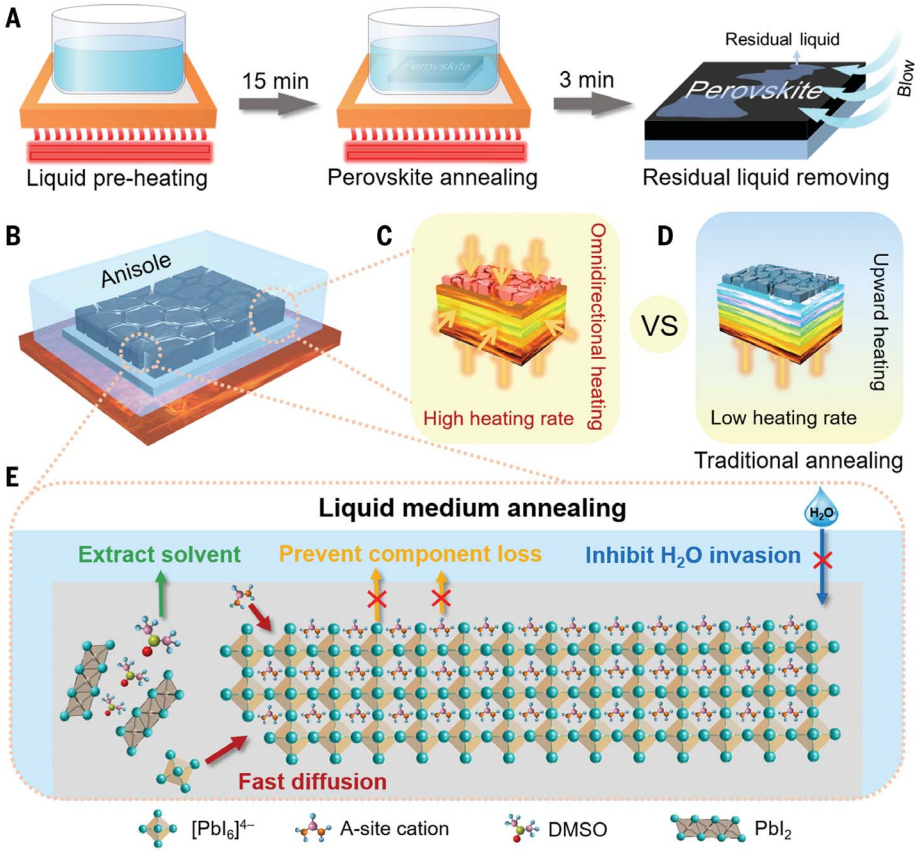

Fig. 1. Diagram of the LMA process. (**A**) The LMA process includes liquid medium preheating, perovskite annealing, and removal of residual liquid. (**B**) LMA illustration with anisole as the liquid medium. (**C** and **D**) Heating direction on perovskite films with the LMA process (omnidirectional heating) (C) and the traditional annealing process (Ref, upward heating) (D). (**E**) Detailed growth dynamics including residual solvent (DMSO) removal and reactant diffusion, as well as preventing volatile component loss and inhibiting moisture invasion using the LMA process.

with most organic solvents (fig. S2 and supplementary text S1). Thus, the residual solvent [e.g., dimethyl sulfoxide (DMSO)] in precursor films can be easily extracted, which potentially provides sufficient reactants to participate in crystal growth. To confirm this, we prepared PbI_2(DMSO) and $MA_2Pb_3I_8{\cdot}2$DMSO intermediate powders (where MA is methylammonium), the major components in precursor films (*24*), to assess the solvent extraction ability of anisole. The relative intensity ratio of PbI_2/PbI_2(DMSO) signals from x-ray diffraction (XRD) measurement is summarized in fig. S3. After immersing PbI_2(DMSO) powder in anisole for 20 min at 20°C, the PbI_2/PbI_2(DMSO) intensity ratio doubled compared with that in air (Fig. 2D). When conducting LMA at 150°C for 10 s, no appreciable PbI_2(DMSO) residue was observed. By contrast, the sample annealed in air retained a considerable amount of PbI_2(DMSO) after heating at 150°C for 10 s. Similar results were observed when annealing $MA_2Pb_3I_8{\cdot}2$DMSO at either 20°C or 150°C (Fig. 2E and fig. S4): LMA resulted in a quicker conversion to $MAPbI_3$. LMA thus improves solvent extraction from solvated intermediate, especially at high temperatures.

To quantify the perovskite film growth rate by LMA, we monitored triple-cation perovskite film growth of $FA_{1-x-y}MA_xCs_yPbI_{3-z}Br_z$ (where FA is formamidinium) in two-step deposition by ex situ ultraviolet–visible spectroscopy. The absorbance at 780 nm was used as an indicator for perovskite formation. The LMA sample exhibited an overall higher absorbance than Ref at the same time in the range of 40 to 100°C (fig. S5). The change of absorbance was plotted as a function of time to obtain the growth rate (k) at each temperature (fig. S5 and supplementary text S2). LMA led to a significantly larger k than that of Ref (Fig. 2F), and the rate difference (Δk) increased with temperature (from 5.49×10^{-4} s^{-1} at 40°C to 1.28×10^{-2} s^{-1} at 100°C; Fig. 2F, inset).

LMA resulted in a substantially different film morphology and quality. Scanning electron microscopy (SEM) images revealed that LMA-prepared perovskite film had a larger grain size of 2.25 ± 0.66 μm (Fig. 2H and fig. S6B) compared with that of Ref at 0.85 ± 0.25 μm

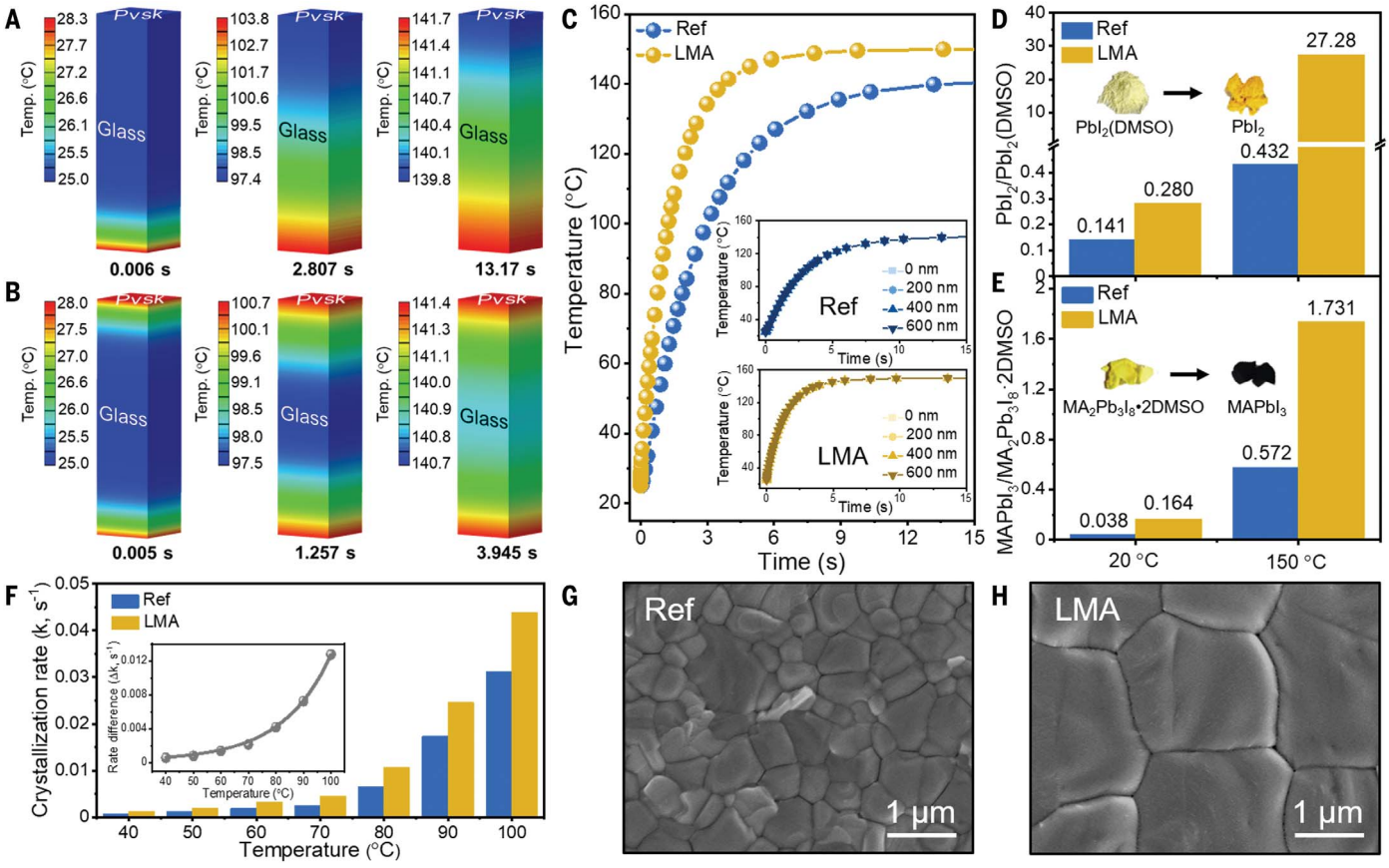

Fig. 2. Crystallization dynamics of perovskites under the Ref and LMA processes. (**A** and **B**) Finite element analysis on the thermal field distribution with annealing time with the Ref process (A) and the LMA process (B). (**C**) Temperature evolution of perovskite film surface with annealing time. Inset: Temperature evolution of perovskite film at different depths. (**D**) Relative content of PbI_2/PbI_2(DMSO) under the Ref and LMA processes at 20°C (for 20 min) or 150°C (for 10 s), expressed as the ratio of the XRD peak areas for the PbI_2 and the PbI_2(DMSO) signals. (**E**) Relative content of $MAPbI_3$/$MA_2Pb_3I_8$·2DMSO under Ref and LMA processes at 20°C (for 20 min) or 150°C (for 10 s), expressed as the ratio of the XRD peak areas for the $MAPbI_3$ and the $MA_2Pb_3I_8$·2DMSO signals. (**F**) Crystallization rate (k) of spin-coated $FA_{1-x-y}MA_xCs_yPbI_{3-z}Br_z$ film under different temperatures (40 to 100°C) calculated from in situ ultraviolet–visible results. Inset: Crystallization rate difference (Δk) between the Ref and LMA processes ($\Delta k = k_{LMA} - k_{Ref}$). (**G** and **H**) Top-view field emission SEM images of $FA_{1-x-y}MA_xCs_yPbI_{3-z}Br_z$ films under the Ref (G) and LMA (H) processes.

(Fig. 2G and fig. S6A). This could be attributed to the accelerated crystal growth rate, which is positively correlated with grain size (*25*). In addition, XRD patterns showed an increased peak intensity of LMA-treated perovskites, suggesting enhanced crystallinity. Moreover, we observed a tenfold increased photoluminescence (PL) intensity and substantially extended carrier lifetime (from 566.32 ns for Ref to 1609.50 ns for LMA; fig. S7), which indicates improved film quality and is in good agreement with the SEM and XRD characterizations.

High-quality perovskite films produced by LMA are likely related to the modulated crystal growth dynamics in the following aspects. First, increased grain size is often achieved at high temperature annealing (*20*), when the grain growth is overwhelmed by promoting the diffusion of reactant. Because of its high heating rate in LMA, precursor films experienced much shorter periods of low temperature (Fig. 2C), which results in enlarged crystal size. Second, during traditional annealing, the wet precursor film preferentially crystallizes from the surface because of solvent evaporation driven by surface tension near the air-liquid interface (*24*, *26*). As a result, residual solvents entrapped underneath the solidified surface are likely to interrupt the construction of perovskite structure (*26*). Moreover, reactive components are prone to react at the air-liquid interface, which changes the stoichiometry of the crystal. During LMA, however, the air-liquid interface is replaced by liquid-liquid contacts, and thus residual solvents are quickly extracted by liquid medium across the entire film thickness. This not only mitigates the disturbance of crystal growth from residual solvents but also prevents undesired side reactions during ambient processing, which leads to polycrystalline films with fewer defects and desired stoichiometry (discussed below). Last, LMA creates a spatially uniform chemical environment by efficient extraction of residual solvents and isolation from ambient conditions and a temporally uniform heat field by fast "top-down" annealing. It further ensures superior uniformity of the resultant films.

Grain boundaries (GBs) in a polycrystalline film usually exhibit different optoelectronic properties from the grain bulk (*27*). LMA results in larger grains in the as-prepared film, which reduces the GBs and improves the absorber uniformity with respect to their optoelectronic characteristics. As evidenced by scanning Kelvin probe microscopy measurement, LMA-treated perovskite films exhibited smaller distribution, with a surface potential difference of ~25 mV (10 × 10 μm^2 area), whereas that of Ref was >40 mV (Fig. 3, A and B). The uniform distribution of surface potential found in LMA samples is beneficial for effective photocarriers extraction in a layer-stacked PSCs to avoid potential recombination. The PL-mapping measurements were performed in the 50 × 50 μm^2 region (fig. S8

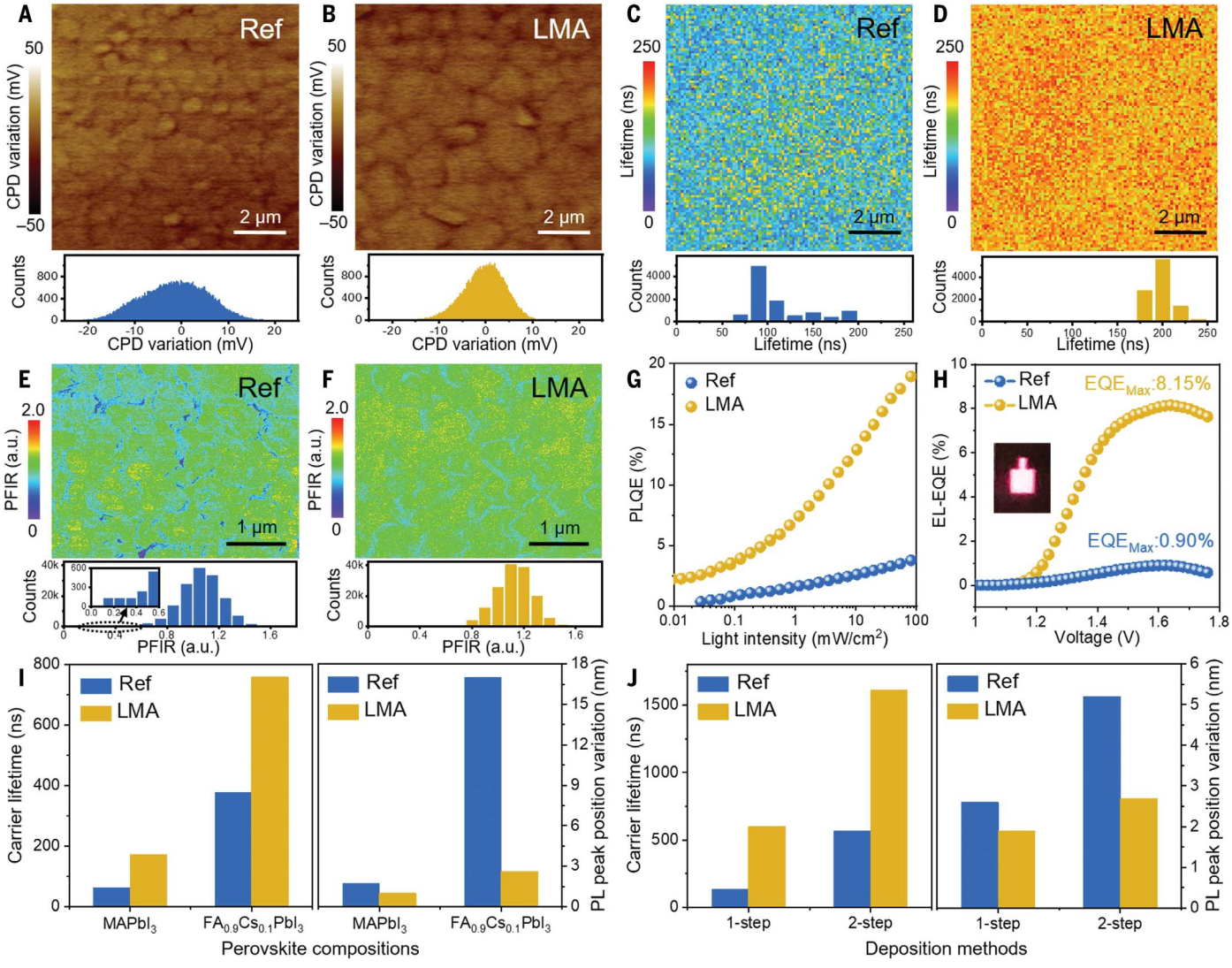

Fig. 3. Uniformity and defect behavior of $FA_{1-x-y}MA_xCs_yPbI_{3-z}Br_z$ films under the Ref and LMA processes and the universality of LMA technology. (**A** and **B**) Surface potential images measured by scanning Kelvin probe microscopy of the Ref- and LMA-fabricated perovskite films. (**C** and **D**) Time-resolved photoluminescence mapping measurements on the Ref- and LMA-fabricated perovskite films with the carrier lifetime as the target signal. (**E** and **F**) PFIR microscopy at an IR frequency of 1480 cm^{-1} (which is resonant with the C–N stretching absorption of MA^+ ion) of Ref- and LMA-fabricated perovskite films. (**G**) PLQE measurements on the Ref- and LMA-fabricated perovskite films as a function of excitation power. (**H**) EQE curves of EL on the Ref- and LMA-fabricated devices while operating as LEDs. Inset: EL image of the LMA-fabricated devices under 1.6 V bias voltage. (**I** and **J**) Carrier lifetimes (obtained from time-resolved photoluminescence results as a perovskite quality indicator) and PL peak position variation (obtained from PL-mapping statistical results as a perovskite uniformity indicator) of perovskites with different compositions: $MAPbI_3$ and $FA_{0.9}Cs_{0.1}PbI_3$ (I) and perovskites prepared under the one-step spin-coating ($Cs_{0.05}(FA_{0.95}MA_{0.05})_{0.95}Pb(I_{0.95}Br_{0.05})_3$ system) and two-step spin-coating ($FA_{1-x-y}MA_xCs_yPbI_{3-z}Br_z$ system) processes (J).

and supplementary text S3), and the fluorescence lifetime mapping was collected in the $10 \times 10\ \mu m^2$ region of the perovskite films. The overall lifetime of LMA (average 196.04 ns) was significantly higher than that of Ref (109.29 ns; Fig. 3, C and D), and the lifetime distribution of LMA was concentrated in the range of ~180 to 240 ns, whereas the Ref exhibited a much broader distribution from 30 to 190 ns.

In traditional annealing, the volatile and chemically reactive components such as MA^+/FA^+ and I^- can easily evaporate or react with ambient molecules (e.g., H_2O, O_2, etc.) (*28*), which causes local element loss and non-stoichiometry at the film surface (*22*). The liquid medium creates a robust microenvironment in which to inhibit volatile component evaporation from desired stoichiometry during annealing (Fig. 1E and fig. S9). To demonstrate this, methylammonium distribution [the infrared frequency of 1480 cm^{-1} represents the C–N stretching (ν_{C-N}) absorption of the MA^+ ion] was probed by peak force infrared (PFIR) microscopy (Fig. 3, E and F). The results showed that LMA-prepared perovskites exhibited an overall slightly increased IR response compared with the Ref sample, along with the more concentrative signal distribution without local low-signal regions (blue regions in Fig. 3E). Stronger IR signal represents better preservation of organic components in the film (*29*), which indicates that LMA could protect this volatile component from escaping to produce more uniform component distribution.

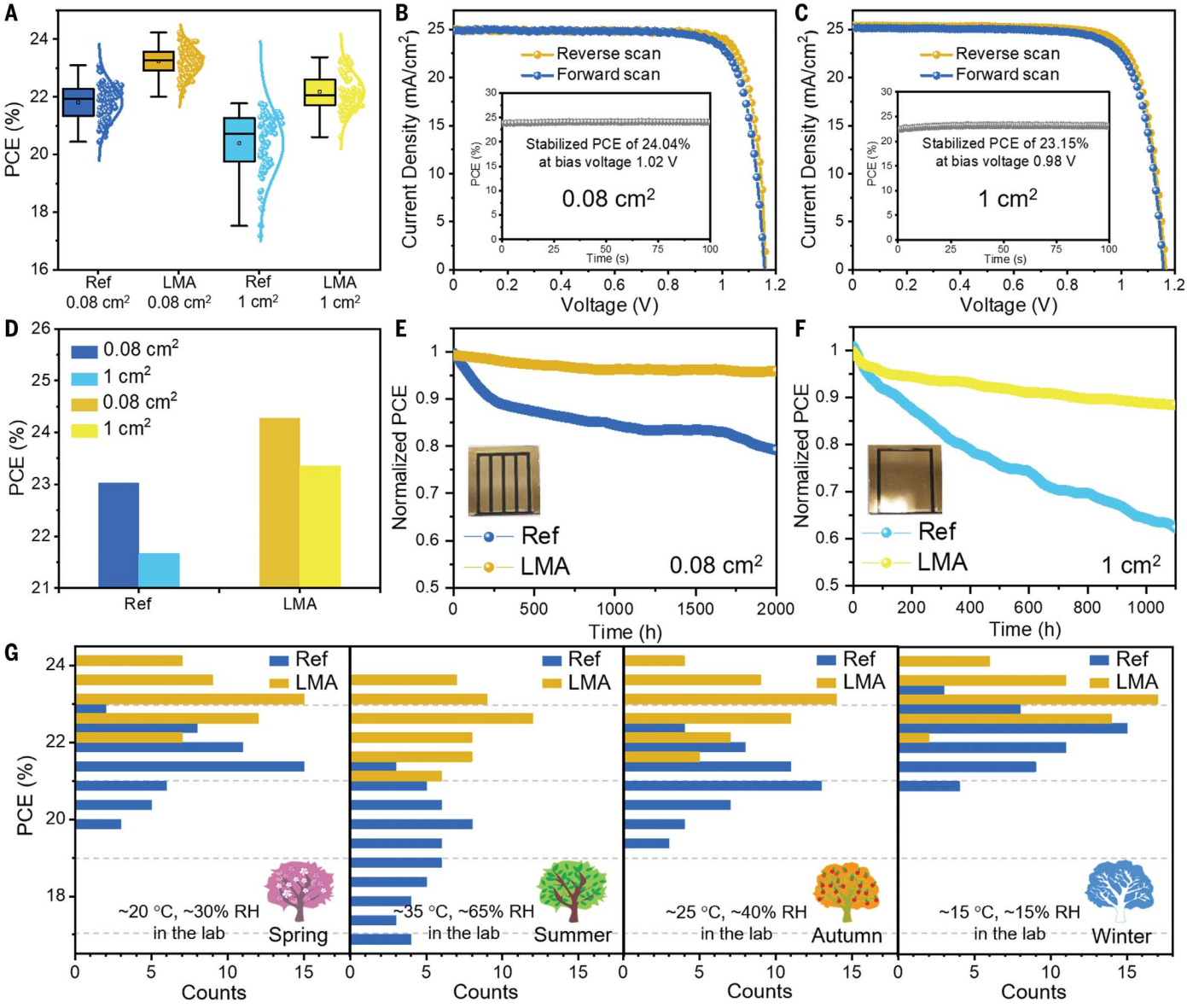

Fig. 4. Optoelectronic performance and stability of $FA_{1-x-y}MA_xCs_yPbI_{3-z}Br_z$–based PSCs prepared under the Ref and LMA processes. (**A**) PCE distribution of 100 individual PSC devices (aperture area of 0.08 cm^2) and 80 individual PSC devices (aperture area of 1 cm^2) fabricated under the Ref and LMA processes, respectively. (**B** and **C**) *J*–*V* curves with reverse (1.2 V to −0.2 V) and forward (−0.2 V to 1.2 V) scan of LMA devices with aperture areas of 0.08 cm^2 (B) and 1 cm^2 (C). Inset: Stabilized PCE at the maximum power point tracking under 1.02 V (B) or 0.98 V (C) bias. (**D**) PCE comparison of the best-performing 0.08-cm^2 PSC and 1-cm^2 PSC under the Ref and $FA_{1-x-y}MA_xCs_yPbI_{3-z}Br_z$ LMA processes, respectively. (**E** and **F**) Evolution of normalized PCEs of Ref and LMA devices with aperture area of 0.08 cm^2 (E) and 1 cm^2 (F) under continuous light irradiation and SPO tracking with a white LED lamp at 100 mW cm^{-2} in a nitrogen atmosphere. (**G**) PCE distribution of Ref- and LMA-fabricated PSCs under different seasons (the average temperature/humidity in the laboratory for spring, summer, autumn, and winter were ~20°C/~30% RH, ~35°C/~65% RH, ~25°C/~40% RH, and ~15°C/~15% RH, respectively).

We also performed x-ray photoelectron spectroscopy (XPS) measurements to examine I^-_{3d} and Pb^{2+}_{4f} signals from corresponding perovskite films. The LMA sample exhibited the same binding energy with respect to I^-_{3d} and Pb^{2+}_{4f} peaks as that of Ref (fig. S10A). However, the I/Pb ratio in the LMA perovskite was 2.92, whereas that in Ref was only 2.74 (fig. S10B). This means that the I^- ions are largely preserved during LMA, resulting in a more stoichiometric structure to alleviate the formation of vacancy defects. We also probed XPS mapping in an area of 50 × 50 μm^2 and found that the binding energy variation of perovskite I^- and Pb^{2+} ions was reduced by LMA (fig. S11 and supplementary text S3). Therefore, LMA has great potential to produce spatially uniform perovskite films, which is beneficial for the scalable fabrication of larger-aperture area PSCs with improved efficiency and stability.

We have revealed that LMA leads to the improved crystallinity and spatial uniformity of component and/or chemical distribution in the resultant films, which corresponds to the defect behavior that determines the corresponding device performance. We first performed PL quantum efficiency (PLQE) measurements on the perovskites at different light intensities (Fig. 3G). The LMA-treated sample exhibited a higher PLQE of 19.6% compared with Ref

(4.0%) under 100 mW/cm^2 irradiation. In addition, its PLQE increased more rapidly with enhancing laser intensity, indicating that the nonradiative recombination centers were more quickly filled (*30*, *31*). PLQE also allows the perovskite solar cells to operate as light-emitting diode (LED) devices. The electroluminescence (EL) signal appeared at a low applied voltage of ~1.1 V, with the emission peak located at ~800 nm, which is consistent with other reports (*32*) (fig. S12). The maximum external quantum efficiency (EQE) reached 8.15% for an LMA-based device at 1.6 V bias voltage, whereas Ref only obtained 0.90% (Fig. 3H). This result shows that the defects related to nonradiative losses in the perovskite absorber were significantly suppressed by the LMA process. Moreover, temperature-dependent PL emission, transient photovoltage and photocurrent decays, and space-charge-limited current measurements (figs. S13 to S16 and supplementary text S4) further confirmed the lower charge carrier recombination rate and improved carrier transport and extraction in the LMA-fabricated device.

We extensively applied the LMA process to other perovskite systems (e.g., $MAPbI_3$ and $FA_{0.9}Cs_{0.1}PbI_3$) and observed improved crystallinity and grain size (fig. S17 and supplementary text S5), as well as marked enhancement of carrier lifetime in LMA samples (Fig. 3I). The spatial uniformity of different perovskite systems was also characterized by PL mapping measurements (fig. S18 and supplementary text S5). Variations in PL emission peak positions were all reduced with the LMA process (Fig. 3I), indicating the uniform composition distribution of LMA samples regardless of perovskite system. We also found that LMA is feasible for one-step deposition to achieve improved carrier lifetime and reduced variation in PL peak positions (Fig. 3J), which leads to improvements in other optoelectronic properties (fig. S20 and supplementary text S6). Finally, to illustrate the applicability of LMA technology on larger-scale perovskite films, we fabricated perovskite films ($FA_{1-x-y}MA_xCs_yPbI_{3-z}Br_z$, 6×6 cm^2) and found that their quality and uniformity could also be improved by LMA (figs. S22 to S25 and supplementary text S7). From these results, we conclude that LMA technology can be universally applied to the fabrication of uniform perovskite films with high quality.

We then fabricated perovskite solar devices (ITO/SnO_2/ $FA_{1-x-y}MA_xCs_yPbI_{3-z}Br_z$/Spiro-OMeTAD/Au) using LMA to investigate their photovoltaic performance. Statistical analyses on 100 individual devices for each condition were summarized. Both the open-circuit voltage (V_{OC}) and the short-circuit current density (J_{SC}) of PSCs were slightly improved by LMA (average V_{OC} of 1.151 V and J_{SC} of 24.66 mA/cm^2 compared with Ref at 1.145 V, 24.52 mA/cm^2, respectively), which was consistent with the corresponding EQE measurements (fig. S29), whereas the fill factor (FF) was substantially enhanced from 77.58 to 81.18% on average (fig. S30). The improved photovoltaic parameters could be attributed to higher crystallinity and fewer defects in LMA-prepared perovskite films. The corresponding PCE achieved 23.24% on average compared with Ref at 21.80% (Fig. 4A). The best device (with an aperture area of 0.08 cm^2) gave a stabilized power output of 24.04% (with a reverse scan PCE of 24.27% and a forward scan PCE of 23.17%; Fig. 4B) and obtained a certified power output of 23.7% under steady-state tests at maximum power point (fig. S31).

LMA leads to uniform perovskite films, which is expected to be beneficial for large-area devices. We fabricated devices with a 1 cm^2 active area based on the same perovskite composition and device architecture. The V_{OC} and J_{SC} of the LMA device (1.155 V and 24.38 mA/cm^2 on average, respectively) and Ref (1.152 V and 24.47 mA/cm^2 on average, respectively) showed similar trends with corresponding small-area devices (fig. S32). When the FF for Ref was reduced to 72.42%, that for LMA achieved 78.54% on average, closer to that of the corresponding small-area devices. It has been reported that FF is reduced with increases in the device area (*6*, *33*, *34*), likely because of the increase of parasitic resistive losses. LMA leads to excellent film uniformity in large areas, which provides large shunting resistance and small series resistance over the entire thin film device (fig. S33). As a result, the LMA-fabricated large-area PSCs exhibited an average PCE of 22.17% (obtained from 80 individual devices), whereas that of Ref was 20.38% (Fig. 4A).

The best LMA device (with an aperture area of 1 cm^2) gave a stabilized power output of 23.15% (with a reverse scan PCE of 23.35% and a forward scan PCE of 22.54%; Fig. 4C) and yielded a certified PCE of 22.3% (average value from a reverse scan PCE of 22.6% and a forward scan PCE of 22.0%) (fig. S34). To our knowledge, this PCE is the highest ever reported for a 1-cm^2 device. The efficiency difference of the best-performing cell between the small (~0.1 cm^2) and large (1 cm^2) area was reduced from 1.37% (Ref sample; tables S8 and S9) to 0.92% (LMA sample; Fig. 4D), and is the smallest reported thus far (fig. S35), which implies promising potential for the scalable fabrication of perovskite solar cells by LMA.

To investigate the stability of the resultant devices with the desired composition, the performance evolution under different kinds of stressors was monitored. The thermal stability test (stored at 85°C under nitrogen atmosphere following the ISOS-D-2I protocol) was performed first. LMA devices retained 95.2% of their initial PCE after 2184 hours of aging, whereas Ref retained 75.8% (fig. S36). In addition, we investigated the operational stability of unencapsulated devices at one-sun LED irradiation with SPO tracking in a nitrogen atmosphere. This revealed that the LMA device only experienced a 5% PCE loss after 2000 hours of aging, whereas a PCE loss of up to 20% was found in Ref (Fig. 4E). According to the degradation mechanisms of PSCs during operation (*10*), high-crystallinity perovskites with ideal stoichiometry and fewer GBs in the film are beneficial for suppressing ion and defect migration, which prolongs the operational lifetime of the device. We also monitored the operational lifetime of 1-cm^2 PSC devices. Although the Ref devices suffered aggravated PCE reduction of up to 39% after 1120 hours of aging, LMA devices only exhibited 10% PCE loss (Fig. 4F). Perovskite films with fewer defects and high uniformity largely reduce the degradation sites at the initial state, which extends the operational lifetime of the corresponding devices profoundly. Therefore, perovskites produced by LMA have a great potential to be adopted in larger-area solar devices with enhanced efficiency and lifetime.

In general, reproducible processing under variable ambient conditions is one of the primary criteria for the commercialization of perovskite PV to ensure low manufacturing costs. However, perovskite has been demonstrated to be moisture sensitive, which causes variations in performance when fabricated at different humidity levels (*15*, *35*, *36*). Even when annealing perovskites in moisture-free surroundings (e.g., in the glove box), the crystal quality can be significantly influenced by various volatile organic compounds. (*16*) Instead of laboriously and expensively controlling the annealing atmosphere, the LMA method is less dependent on the fabrication climate (in-house) because of the robust microenvironment created by the liquid medium. We also investigated its reproducibility under all-weather in-house conditions. The perovskite solar cells ($FA_{1-x-y}MA_xCs_yPbI_{3-z}Br_z$ as absorber) were fabricated in four quarters with varied humidity in the laboratory (the average temperature/humidity for spring, summer, autumn, and winter were ~20°C/~30% RH, ~35°C/~65% RH, ~25°C/~40% RH, and ~15°C/~15% RH, respectively). The traditional annealing method was strongly dependent on weather, resulting in an average PCE of >22% in winter and 19% in summer with poor reproducibility. There was no obvious performance difference in LMA devices (fig. S37), with most having a PCE of >23% (Fig. 4G) because of the liquid medium, which effectively blocks interference from the ambient conditions (Fig. 1E). This result shows the all-weather adaptability of LMA technology for the widespread fabrication of perovskite photovoltaics.

We also fabricated solar cells with different perovskite compositions (e.g., $MAPbI_3$, $FA_{0.9}Cs_{0.1}PbI_3$, and $FASn_{0.5}Pb_{0.5}I_3$) and multiple processing (e.g., one-step spin-coating) to determine the generality of LMA technology. The LMA process was associated with a noticeable performance improvement (fig. S19, S21, and S27 and supplementary text S5, S6, and S8). Furthermore, the liquid medium can be expanded from anisole to trichlorobenzene and Dowtherm A (fig. S38), for example, highlighting the extensive opportunities to further improve LMA technology for perovskite thin film fabrication.

REFERENCES AND NOTES

1. S. Xie *et al*., *Appl. Sci.* **10**, 4285 (2020).
2. F. P. García de Arquer, A. Armin, P. Meredith, E. H. Sargent, *Nat. Rev. Mater.* **2**, 16100 (2017).
3. A. Kojima, K. Teshima, Y. Shirai, T. Miyasaka, *J. Am. Chem. Soc.* **131**, 6050–6051 (2009).
4. H. Zhou *et al*., *Science* **345**, 542–546 (2014).
5. A. Al-Ashouri *et al*., *Science* **370**, 1300–1309 (2020).
6. M. Jeong *et al*., *Science* **369**, 1615–1620 (2020).
7. M. Green *et al*., *Prog. Photovolt. Res. Appl.* **29**, 3–15 (2021).
8. N. K. Tailor *et al*., *J. Mater. Chem. A Mater. Energy Sustain.* **8**, 21356–21386 (2020).
9. X. Niu, N. Li, Q. Chen, H. Zhou, *Adv. Energy Sustain. Res.* **2**, 2000046 (2020).
10. N. Li, X. Niu, Q. Chen, H. Zhou, *Chem. Soc. Rev.* **49**, 8235–8286 (2020).
11. N. Li *et al*., *Joule* **4**, 1743–1758 (2020).
12. J.-P. Correa-Baena *et al*., *Science* **363**, 627–631 (2019).
13. T. Zhang *et al*., *Sci. Bull. (Beijing)* **64**, 1608–1616 (2019).
14. L. Li *et al*., *ACS Nano* **11**, 8804–8813 (2017).
15. J. You *et al*., *Appl. Phys. Lett.* **105**, 183902 (2014).
16. J. Huang *et al*., *ACS Appl. Mater. Interfaces* **8**, 21505–21511 (2016).
17. H. Hu *et al*., *J. Mater. Chem. A Mater. Energy Sustain.* **8**, 1578–1603 (2020).
18. N. J. Jeon *et al*., *Nat. Mater.* **13**, 897–903 (2014).
19. C. Bi *et al*., *Nat. Commun.* **6**, 7747 (2015).
20. M. Kim *et al*., *ACS Nano* **11**, 6057–6064 (2017).
21. Y. Yang *et al*., *Sci. Rep.* **7**, 46724 (2017).
22. Y. Deng *et al*., *Joule* **4**, 1949–1960 (2020).
23. G. Divitini *et al*., *Nat. Energy* **1**, 15012 (2016).
24. S. Chen *et al*., *Sci. Adv.* **7**, eabb2412 (2021).
25. L. Li *et al*., *Adv. Mater.* **28**, 9862–9868 (2016).
26. W. Qian *et al*., *Matter* **4**, P942–P954 (2021).
27. J.-W. Lee *et al*., *Mater. Today Energy* **7**, 149–160 (2018).
28. Z. Song *et al*., *J. Phys. Chem. Lett.* **9**, 6312–6320 (2018).
29. D. S. Jakob *et al*., *Angew. Chem. Int. Ed. Engl.* **59**, 16083–16090 (2020).
30. Y. Chen *et al*., *Nat. Commun.* **10**, 1112 (2019).
31. C. M. Sutter-Fella *et al*., *Nano Lett.* **16**, 800–806 (2016).
32. G. C. Dousmanis, C. W. Mueller, H. Nelson, K. G. Petzinger, *Phys. Rev.* **133** (1A), A316–A318 (1964).
33. W. S. Yang *et al*., *Science* **356**, 1376–1379 (2017).
34. G. Kim *et al*., *Science* **370**, 108–112 (2020).
35. L. Contreras-Bernal *et al*., *ACS Sustain. Chem.& Eng.* **8**, 7132–7138 (2020).
36. Y. Xu *et al*., *ChemPhysChem* **17**, 112–118 (2016).

ACKNOWLEDGMENTS

We thank J. Song and Y. Lu (Beijing University of Technology) for discussions about crystal growth dynamics and W. Zhou and Y. Jiang (Peking University) for assistance with fabricating perovskite solar cells. **Funding:** This work was supported by the National Key Research and Development Program of China (grant nos. 2020YFB1506400 and 2017YFA0206701), the National Natural Science Foundation of China (grant nos. 51972004, 21975028, and 22005035), the Natural Science Foundation of Beijing, China (grant no. JQ19008), Beijing Municipal Science and Technology Project (Z181100005118002), the China Postdoctoral Science Foundation (grant nos. 2020TQ0043 and 2020M680012), and the Tencent Foundation through the XPLORER PRIZE. **Author contributions:** H. Zhou, Q.C., N.L., X.N., and L.L. conceived the idea. H. Zhou, Q.C., N.L., and X.N. designed the experiments. N.L. and X.N. were involved in all experiments. H.W. performed the finite element analysis. X.L. contributed to the scheme design. Z.G. helped with the EL measurements. G.L. performed the transient photocurrent and transient photovoltage measurements. H.C. and J.W. conducted the PLQE measurements. Y.L., X.W., and J.H. performed the SKPM measurements. H.X. performed the XPS measurement. D.S.J. and X.G.X. conducted the peak force infrared measurements. Z.H., X.Z., Y.C., Y.Z. C.Z., H. Zai, Y.B., S.M., H.L., and R.F. contributed to the fabrication of high-performance perovskite solar cells. H. Zhou, Q.C., N.L., and X.N. wrote and revised the manuscript. All authors were involved in discussions of data analysis and commented on the manuscript. **Competing interests:** The authors declare no competing interests. **Data and materials availability:** All data are available in the main text or the supplementary materials.

SUPPLEMENTARY MATERIALS

science.sciencemag.org/content/373/6554/561/suppl/DC1
Materials and Methods
Supplementary Text S1 to S8
Figs. S1 to S39
Tables S1 to S12
References (*37*–*62*)
MDAR Reproducibility Checklist

5 March 2021; accepted 28 June 2021
10.1126/science.abh3884

Science

Liquid medium annealing for fabricating durable perovskite solar cells with improved reproducibility

Nengxu LiXiuxiu NiuLiang LiHao WangZijian HuangYu ZhangYihua ChenXiao ZhangCheng ZhuHuachao ZaiYang BaiSai MaHuifen LiuXixia LiuZhenyu GuoGuilin LiuRundong FanHong ChenJianpu WangYingzhuo LunXueyun WangJiawang HongHaipeng XieDevon S. JakobXiaoji G. XuQi ChenHuanping Zhou

Science, 373 (6554), • DOI: 10.1126/science.abh3884

Evening out the heat

The conversion of precursors into the active layer of perovskite solar cells normally occurs by heating the underlying substrate. Conversion tends to occur near the top of the film, where solvent is lost, and unwanted preheating of reactants occurs near the substrate before the reaction. Li *et al*. show that the use of a surrounding heat transfer oil (anisole) leads to more rapid and even heating, removes solvent, and avoids air and water contamination effects. The larger grains and more uniform films led a much greater retention of efficiency in moving from small-area to large-area devices. —PDS

Science (ISSN) is published by the American Association for the Advancement of Science. 1200 New York Avenue NW, Washington, DC 20005. The title *Science* is a registered trademark of AAAS.